ISSN 1674-1056
http://cpb.iphy.ac.cn
http://iopscience.iop.org/cpb
中国物理 B
Chinese Physics
中国物理 Chinese Physics B

Short-wave infrared InGaAs photodetectors and focal plane arrays

Yong-Gang Zhang(张永刚), Yi Gu(顾溢), Xiu-Mei Shao(邵秀梅), Xue Li(李雪), Hai-Mei Gong(龚海梅), Jia-Xiong Fang(方家熊)

Citation: Chin. Phys. B . 2018, 27(12): 128102. **doi:** 10.1088/1674-1056/27/12/128102
Journal homepage: http://cpb.iphy.ac.cn; http://iopscience.iop.org/cpb

What follows is a list of articles you may be interested in

Effects of growth conditions on optical quality and surface morphology of InGaAsBi

Jia-Kai Li(李家恺), Li-Kun Ai(艾立鹍), Ming Qi(齐鸣), An-Hui Xu(徐安怀), Shu-Min Wang(王庶民)
Chin. Phys. B . 2018, 27(4): 048101. **doi:** 10.1088/1674-1056/27/4/048101

Effects of proton irradiation at different incident angles on InAlAs/InGaAs InP-based HEMTs

Shu-Xiang Sun(孙树祥), Zhi-Chao Wei(魏志超), Peng-Hui Xia(夏鹏辉), Wen-Bin Wang(王文斌), Zhi-Yong Duan(段智勇), Yu-Xiao Li(李玉晓), Ying-Hui Zhong(钟英辉), Peng Ding(丁芃), Zhi Jin(金智)
Chin. Phys. B . 2018, 27(2): 028502. **doi:** 10.1088/1674-1056/27/2/028502

Performance of dual-band short- or mid-wavelength infrared photodetectors based on InGaAsSb bulk materials and InAs/GaSb superlattices

Yao-yao Sun(孙姚耀), Yue-xi Lv(吕粤希), Xi Han(韩玺), Chun-yan Guo(郭春妍), Zhi Jiang(蒋志), Hong-yue Hao(郝宏玥), Dong-wei Jiang(蒋洞微), Guo-wei Wang(王国伟), Ying-qiang Xu(徐应强), Zhi-chuan Niu(牛智川)
Chin. Phys. B . 2017, 26(9): 098506. **doi:** 10.1088/1674-1056/26/9/098506

Physical modeling based on hydrodynamic simulation for the design of InGaAs/InP double heterojunction bipolar transistors

Ge Ji,Liu Hong-Gang,Su Yong-Bo,Cao Yu-Xiong,Jin Zhi
Chin. Phys. B . 2012, 21(5): 058501. **doi:** 10.1088/1674-1056/21/5/058501

Step instability of the $In_{0.2}Ga_{0.8}As$ (001) surface during annealing

Zhang Bi-Chan,Zhou Xun,Luo Zi-Jiang,Guo Xiang,Ding Zhao
Chin. Phys. B . 2012, 21(4): 048101. **doi:** 10.1088/1674-1056/21/4/048101

TOPICAL REVIEW — Photodetector: Materials, physics, and applications

Short-wave infrared InGaAs photodetectors and focal plane arrays*

Yong-Gang Zhang(张永刚)[1,2,†], Yi Gu(顾溢)[1,2], Xiu-Mei Shao(邵秀梅)[1], Xue Li(李雪)[1], Hai-Mei Gong(龚海梅)[1], and Jia-Xiong Fang(方家熊)[1]

[1] *Key Laboratory of Infrared Imaging Materials and Detectors, Shanghai Institute of Technical Physics, Chinese Academy of Sciences, Shanghai* 200083, *China*

[2] *State Key Laboratory of Functional Materials for Informatics, Shanghai Institute of Microsystem and Information Technology, Chinese Academy of Sciences, Shanghai* 200050, *China*

(Received 6 September 2018; revised manuscript received 21 September 2018; published online 10 November 2018)

In this article, unique spectral features of short-wave infrared band of 1 μm–3 μm, and various applications related to the photodetectors and focal plane arrays in this band, are introduced briefly. In addition, the different material systems for the devices in this band are outlined. Based on the background, the development of lattice-matched and wavelength-extended InGaAs photodetectors and focal plane arrays, including our continuous efforts in this field, are reviewed. These devices are concentrated on the applications in spectral sensing and imaging, exclusive of optical fiber communication.

Keywords: InGaAs, short-wave infrared, photodetectors, focal plane arrays

PACS: 81.05.Ea, 85.60.Dw, 72.40.+w, 81.15.Hi **DOI:** 10.1088/1674-1056/27/12/128102

1. Introduction

Photodetectors (PDs) and focal plane arrays (FPAs) responding to 1 μm–3 μm short-wave infrared (SWIR) wavelength band have attracted much attention because of their unique spectral features in this band. For example, the water molecules, which are the most important component on the earth, have four important absorption zones around 2.7, 1.9, 1.4, and 1.1 μm, respectively. Clear transmission windows exist between them, as shown in Fig. 1. The high contrast characteristics in SWIR band make it fascinating to observe this planet from satellite to obtain diverse information. On the ground, fog penetrating and special night vision, and also astronomy in this band are required. Furthermore, the spectroscopic character of numerous water containing substances such as soil, fruits, beverage, and medicament in SWIR band also arouse much interest. Besides, CO_2 also has significant spectral fingerprints in this band, especially those around 1.6 μm and 2.1 μm. These absorption features are located in the water absorption windows with distinct intensities, which makes them quite suitable for CO_2 distribution mapping or monitoring from space or on ground. Meanwhile, many areas including spectra of characteristic absorption of gases or liquids, water content in soil, crop yield estimation, cloud and mineral discrimination, thermal photovoltaic energy conversion, thermal imaging of high temperature objects, wind detection lidar, and so on are also presumed to rely on PDs and FPAs in this band.

Quantum- or photon-type PDs and FPAs have different types, such as photo-conductor or photovoltaic. For the applications mentioned above, photovoltaic-types are more preferable because the devices can operate at zero bias, resulting in lower dark current. In the SWIR band, these types of devices mainly rely on two kinds of semiconductor materials; *i.e.*, II–VI and III–V. The HgCdTe (MCT), a representative variable gap semiconductor of II–VIs, has worked successfully in SWIR band.[1] This can be epitaxially grown on a lattice-matched but quite expensive CdZnTe substrate, and excellent performances of the devices have been achieved. However, motivations to replace MCT especially in SWIR band exist because of some of the technological problems of this material. The most important reason is the weak Hg–Te bonds in MCT material, which results in instabilities of the surface, interface and even the bulk material. Some other issues are the difficulties in growing the material and processing the chip at lower temperatures, as well as operating at lower operating temperature and weakening the radiation hardness of the devices. In III–Vs, the antimonides that form some lattice-matched systems also cover the SWIR band. The binary InAs and GaSb show nearly the same lattice constant around 6.1 Å, while different systems (such as quaternary InAsPSb or InGaAsSb) could grow on these substrates. The quaternary InAsPSb on InAs substrate covers the bandgap from InAs of 0.36 eV to about 0.7 eV (considering the miscibility gap) at 300 K, and matches the SWIR band perfectly. For example, in this system the liquid phase epitaxy (LPE) grown SWIR PDs has previously been demonstrated.[2–4] The difficulty in

*Project supported by the National Key Research and Development Program of China (Grant No. 2016YFB0402400), the National Natural Science Foundation of China (Grant Nos. 61675225, 61605232, and 61775228), and the Shanghai Rising-Star Program, China (Grant No. 17QA1404900).

†Corresponding author. E-mail: ygzhang@mail.sim.ac.cn

© 2018 Chinese Physical Society and IOP Publishing Ltd

simultaneously controlling the three group-V elements As, P, and Sb makes the growth of device-quality wafers by using the metal–organic–vapor phase epitaxy (MOVPE) or molecular beam epitaxy (MBE) challenging. The other lattice-matched antimonide quaternary system of InGaAsSb on GaSb, which covers the bandgap from InAs rich corner of 0.283 eV to GaSb rich corner of 0.727 eV at 300 K, also matches the SWIR band quite well. For example, on this system LPE,[5] MOVPE,[6] and solid source molecular beam epitaxy (SSMBE)[7,8] grown SWIR PDs have been demonstrated. The response wavelength of type-II quantum wells based on antimonide also touches this band.[9,10] In an antimonide system, no limitation exists in theory, but in practice the difficulties in treating the Sb containing materials in both epitaxy and chip processing aspects still exist. Compared with an InP substrate, the obtaining of high-quality GaSb substrates at moderate price is still an issue, whereas the non-transparent InAs substrate in this band also limit its application, especially for two-dimensional (2D) FPAs.

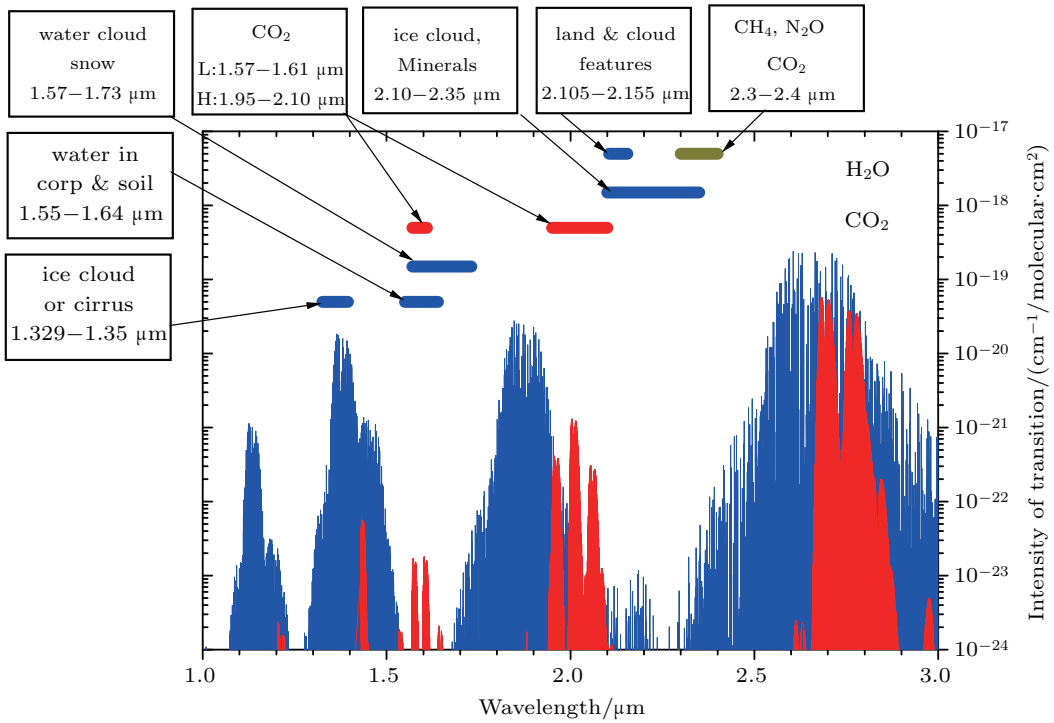


Fig. 1. (color online) Spectral features of SWIR band, including absorption intensities of H_2O and CO_2 and showing main observation wavelength zones of different objects from satellites.

In addition to MCT or antimonide materials, the III–V ternary $In_xGa_{1-x}As$ is a good candidate to cover the SWIR band (see Figs. 2 and 3). The $In_xGa_{1-x}As$, namely the alloy of two direct bandgap binaries, covers the whole bandgap range of 0.36 eV of InAs to 1.43 eV of GaAs with direct bandgap in full region. At indium composition x of 0.53, it is lattice-matched to InP substrate with a bandgap about 0.75 eV at 300 K. The PD adopting this composition has a cutoff wavelength of about 1.7 μm, namely lattice-matched device, which has been sufficiently developed for decades and widely used in optical fiber communication of 1.31 μm or 1.55 μm wavelengths, its performance has proved to be excellent. For the ternary $In_xGa_{1-x}As$ of x from 0.53 to 1, the bandgap could be varied from 0.75 eV to 0.36 eV at 300 K, corresponding to cutoff wavelength ranging from 1.7 μm to 3.4 μm, which fits the long side of SWIR band very well. Therefore, to shift the response to longer wavelength, the indium content in the InGaAs alloy should be increased. For instance, to move the cutoff wavelength of the device grown on an InP substrate from 1.7 μm to about 2.5 μm, the indium content in InGaAs alloy must be increased from 53% to about 83%, which introduces quite a large lattice mismatch of about +2% between InGaAs epitaxial layer and InP substrate, in this case an extraordinary buffer layer should be inserted in between to prevent the material quality from excessively degrading. Meanwhile, the full maturity of the growth and processing technology of this material system, which have been validated from mass production, could compensate for the residual degradation caused by adequate mismatch, and thus making this ternary very attractive from the point of view of application. In the lattice-mismatched system of $In_xGa_{1-x}As$ ($x > 0.53$) on InP, or namely wavelength extended devices, some options of buffer materials with different essential points of concern are still present. In this article, the development of lattice-matched and wavelength-extended InGaAs PDs, as well as FPAs, including our continuous efforts in this field, are briefly reviewed. These devices concentrate on spectral sensing and imaging applications, exclusive of optical fiber communica-

tion.

2. Lattice-matched InGaAs PDs and FPAs

The development of lattice-matched InGaAs PDs can be traced to decades ago. Pearsall and Hopson reported the LPE grown InGaAs material and PDs in the 1970's,[11,12] targeting at optical fiber communication. For optical fiber communication applications where response speeds of PDs are the most important concern, normally the devices work at higher reverse bias to reduce the capacitance. In other words the photovoltaic detectors operate in photoconductive mode. In spectral sensing and imaging applications the sensitivity merit of PDs and FPAs become key points. Because InGaAs is a direct band gap material with higher absorption and mobility, the response speed of the devices should be high enough inherently for conventional spectral sensing and imaging applications. Therefore, the devices are normally work at zero bias to reduce the dark current. In other words, the devices operate in photovoltaic mode.

Owing to sustained progress of optical fiber communication and according to the differences in application scene, lattice-matched InGaAs PDs and FPAs, in a manner of speaking, are developed on existing technologies. As for the appropriative readout integrated circuit (ROIC) design and fabrication, the hybridization of the chip with the ROIC and exquisite packaging, existing technologies from MCT and other devices could also be customized into InGaAs FPAs. This has accelerated the development of lattice-matched InGaAs PDs and FPAs for spectral sensing and imaging purpose when real demands appear. For example, in 2007, Onat *et al.* reported MOVPE grown 640×512 FPA of 20-μm pitch with a dark current density of 2 nA/cm^2 at −100-mV bias and temperature of 12.3 °C,[13] and the device is of planar type. In 2007, Li *et al.* reported gas source molecular beam epitaxy (GSMBE) grown 256×1 FPA of 56 μm×56 μm element sensitive area with R_0A of 5 kΩ·cm^2 at room temperature (RT),[14] the device is of mesa type. In 2009, the FPA format has been raised to 1k×1k reported by MacDougal, *et al.*[15] The MOVPE grown planar-type devices show dark current density below 1.0 nA/cm^2 at −100-mV bias and 7 °C. Here, the planar-type device means that the pn junction is formed through diffusion in processing step, whereas mesa-type device means the the pn junction is formed during epitaxy by in situ doping. With the excellent characteristics of the lattice-matched InGaAs system and related mature technologies, and especially the clear prospect of the FPAs, such devices, including III–V lab and SOFRADIR in France,[16–18] SITP/CAS in China,[19] Fraunhofer IAF in Germany,[20] Aerius Photonics, Raytheon and Spectrolab in USA[21,22] SemiConductor Devices in Israel,[23] and so on, have been developed. For imaging purposes, 640×512 VGA format of 15-μm pitch, which is the most popular version for mass applications, has already matured and become products. An even lager format product of 1280×1024 SXGA format of 10-μm pitch is being developed.

For these InGaAs devices, the lattice matches that of InP substrate, the cutoff wavelength is fixed at about 1.7 μm, but the cut-on wavelength still could be tailored. In the back illuminating case, the cut-on wavelength is determined by the bandgap of InP substrate to be about 0.93 μm, through thinning or removing the InP substrate and tailoring the epitaxial structure, the cut-on wavelength of the FPAs moved to shorter wavelength and entered into visible band, and even decreased down to 400 nm.[13,16–18,23,24] The visible extended version of InGaAs FPAs can partially incorporate the function of Si CCD/CMOS camera into the system, which is desirable for certain applications. Special formats of the device are especially useful for applications in spectral sensing or line scan imaging. For example 2048×1 array with 400-kHz line rate and 6000×8 array of 13-μm pitch on 4″ wafer have been reported by Xenics[25] and Teledyne Judson,[26] respectively. The monolithic integration of multiple narrow band Fabry–Pérot filter on the chip for hyperspectral application in SWIR band has also been demonstrated in SITP/CAS of China.[27] Traditionally, lattice-matched InGaAs is also used for avalanche photodetectors (APDs) of communication band, although their performance is still limited compared with some other material system on the other band. For example, InGaAs 2D FPAs in Geiger mode was also explored by Itzler *et al.*[28] and Baba *et al.*,[29] targeting at the time resolution or lidar applications.

For InGaAs FPAs lattice matched to InP, planar-type devices have been the main stream. In addition to traditional close, semi-close or open tube diffusion with volatilize or spin-on Zn dopants, utilizing the MOVPE chamber to perform the diffusion process deserves to be advocated.[30] In this process, metal–organic source like dimethyl zinc was used as dopant and cracked PH_3 or AsH_3 provides sufficient surface protection, therefore controllability, reproducibility, and uniformity of the diffusion could be improved. Because the dark current density of such devices at RT has decreased down to 1 nA/cm^2 of intrinsic level. In this case, the passivation process have become critical, low stress diffusion mask[31] and optimization of the passivation films[32] remain an issue. Real applications — especially in the space, radiation hardness,[33,34] lifetime,[35] package reliability,[36] and space qualification[37] — of these devices have also been performed in detail.

It should be noticed here that the performance of the devices, such as the dark current, is hypersensitive to operating temperature and bias voltage, and in most case the reachable lowest bias voltage of each FPA's pixel is determined by ROIC's offset voltage. The overall performances of the PDs and FPAs are also inclusive of pre-amplifier or ROIC perfor-

mances, and the coupling parameters (*e.g.*, the elemental and parasitic capacitance) between them. For lattice-matched InGaAs FPAs, the dark currents of the devices have reached a fairly low level, especially at lower operating temperature. Consequently, the overall performance is not presently dominated by the FPA chip but is dominated by the ROIC and coupling parameters in many cases. Furthermore, for FPA, especially of large format, the homogeneity of the pixels determines the system's performance.

3. Wavelength-extended InGaAs PDs and FPAs

Intuitively speaking, lattice-matched systems like MCT or antimonide are more preferable in SWIR band than mismatched system, at least in theory. However, wavelength-extended InGaAs of higher indium content is still a strong competitor in this band, mainly from practical, technological, and even economical points of view, which originate from the accumulation of the growth and processing technologies in this material system, as well as their favorable characteristics.

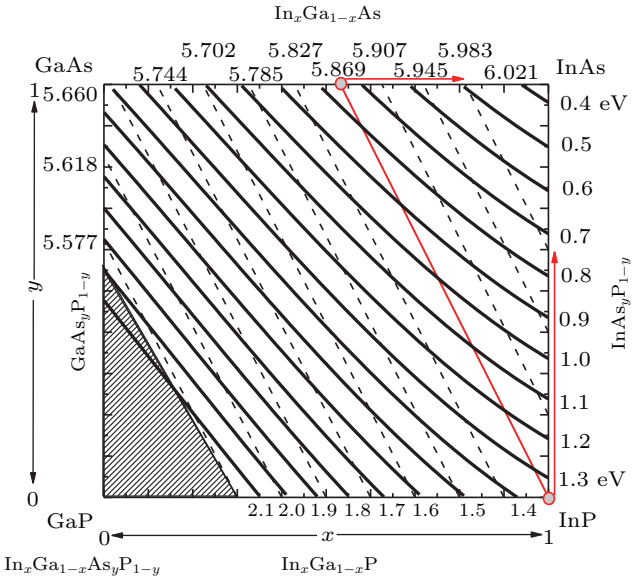


Fig. 2. (color online) Composition-dependent band gap and lattice constant relationship of quaternary $In_xGa_{1-x}As_yP_{1-y}$ system. Solid lines show contours of band gap energy in unit eV, dashed lines refer to contours of lattice constants in unit Å, and four axes represent ternaries of $In_xGa_{1-x}P$, $In_xGa_{1-x}As$, $GsAs_yP_{1-y}$, and $InAs_yP_{1-y}$ respectively. Shadow region represents indirect band zone.

With the higher-indium-content InGaAs serving as the absorption layer, the wavelength-extended InGaAs PDs and FPAs could still be constructed by using different material systems such as InGaAsP (in fact InAsP/InGaAs) or AlGaInAs (in fact InAlAs/InGaAs).[38] The relationships between band gap and lattice constant of the two systems are shown in Figs. 2 and 3, respectively. The wavelength-extended InGaAs PDs have been reported by Martinelli *et al.*[39] and Makita *et al.*[40] in 1988 by using the hydride vapor phase epitaxy (HVPE) in homojunction or heterojunction configurations, respectively. Forte-Poisson *et al.* then reported the MOVPE grown PDs of heterojunction configuration in 1992.[41] Notice that those researches are still motivated in the area of optical communication because the fluoride fiber has much lower loss than silica fiber but at longer wavelength (about 2.5 μm). With the notable development of semiconductor lasers and optical fiber amplifiers and the consideration of frangible features of fluoride fiber, this target seems to be stagnant. However, 10 years later, the sensing and imaging motivations have become interested in a natural extension of lattice-matched devices.

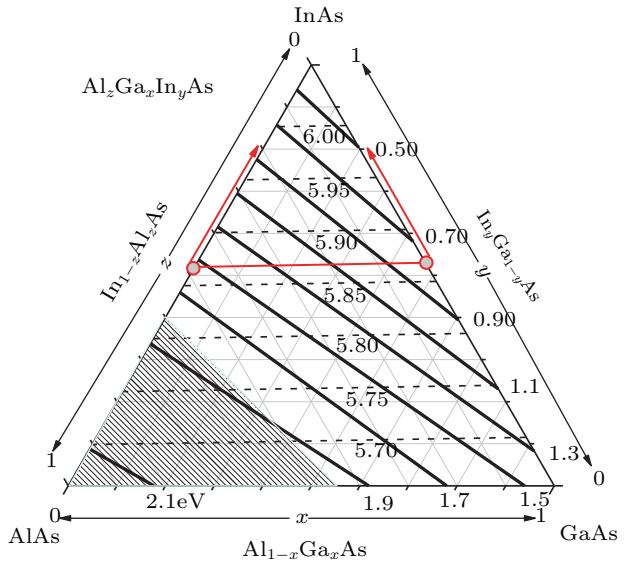


Fig. 3. (color online) Composition-dependent band gap and lattice constant relationship of quaternary $Al_zGa_xIn_yAs$ system. Solid lines show contours of band gap energy in unit eV, dashed lines denote the contours of lattice constants in unit Å, and three axes represent the ternaries of $Al_{1-x}Ga_xAs$, $In_yGa_{1-y}As$, and $In_{1-z}Al_zAs$ respectively. The shadow region refers to indirect band zone.

Many efforts have been made to investigate the wavelength-extended InGaAs PDs and FPAs since the 2000s. The first GSMBE grown homojunction PD was reported in 2005 as a trial of exploration. Its cutoff wavelength was only extended to 1.9 μm.[42] The cutoff wavelengths were extended to 2.2 μm and 2.5 μm,[43] then heterojunction PD using InAlAs as cap and linear graded buffer layer was demonstrated.[44] The longest cutoff wavelength was extended to 2.9 μm and the overall wavelength-dependent performances of the devices were evaluated in detail.[45] Meanwhile, n-on-p configuration of the PD has also been validated,[46] which shows that its performance is better than conventional p-on-n configuration but the mesa becomes higher. For lattice-mismatched devices with thicker active layer, a buffer layer is essential. Generally speaking, the thicker the buffer layer, the better the epitaxy quality is. However, comparing with HVPE or MOVPE, the epitaxial growth rate of MBE is low, normally on the order of 1 μm/hour. Under this practically restrictive condition, the buffer strategy, or using a thinner buffer to reach better effects, are the most important concern. Keeping this in mind, different types of buffer structures have been investigated including linear graded,[47] con-

vex graded,[48] step graded,[49] composition overshoot,[50] and the combinations,[51] and the inserting of digital alloy into the buffer,[52] while total digital graded buffer structures[53] have also been verified. Optimal growth parameters of the buffer have been investigated in detail.[42–53] Generally speaking, linear graded buffer of accredited thickness is suitable for the devices, and the overall effects are acceptable. Inserting more interfaces into the buffer structure has a positive effect on the buffer quality, especially at the beginning of buffer growth, whereas the total thickness of the buffer is still a pivotal factor. In our GSMBE process, the linear grading of the composition, such as of ternary InAlAs buffer with two group III elements, was particularly realized by changing the In and Al source temperature slowly and simultaneously, without shutter operation. This process is easier than the controlling of two or more group V elements, such as in ternary InAsP. Oppositely, open and close the shutters too frequently to reach a thick buffer structure is inadvisable practically. For those lattice-mismatched InGaAs devices, the inserting of electron barriers into the absorption layer is effective to reduce the dark current, as well as to promote overall performances,[54,55] meanwhile the position of inserted electron barriers should be regulated,[56] as should the doping level.[57] During studying this topic, the material parameters such as optical[58] and transportation[59] characteristics of the high-indium-content InGaAs were accumulated, the methods of evaluating material related device performances[60] were validated. From the data analysis of different categories including our work,[61] a rule of thumb denoted as IGA-rule 17[62] to describe the wavelength and operating temperature-dependent performance of lattice-mismatched InGaAs PDs and FPAs in 2 μm–3 μm band was developed, similar to the well-known rule 07 for MCT devices.[63]

Based on our GSMBE grown lattice-mismatched wafers of various FPA structures, wavelength-extended InGaAs FPAs of different formats have been developed at SITP/CAS of China, targeting space spectral applications. The 256×1 linear array was reported in 2007,[64] after that 2D arrays of 64×64[65] and 512×256[66] were reported in 2013 and 2017, respectively. During this period, characteristics and processing of the devices were investigated in detail.[67–74] These devices are of all mesa-type and have a cut-off wavelength around 2.5 μm in p-on-n configuration. Meanwhile, FPAs of mesa-type n-on-p configuration, as well as planar-type diffusion formed pn junction using n-on-n epitaxial wafer were also evaluated.[75] For the wavelength-extended versions of InGaAs FPA, higher mesa of n-on-p configuration was harmful to the passivation especially for FPAs of small pitch. On this lattice-mismatched structures, defects especially punching through dislocations are difficult to avoid totally, which may cause leakage tunnel by the enhanced diffusion for planar processing and this can degrade the performance. In space applications, the radiation hardness of the devices is of concern. The proton irradiation effects have been appraised on GSMBE grown devices,[76] although space evaluation of radiation damage of MOVPE grown devices has previously been reported by Kleipool, *et al.*[77] With the growing of scale in both size and pixel number, the homogeneity of the FPA becomes increasingly important, and even dominates the system performance. Therefore, the uniformity of SWIR InGaAs FPA has been analyzed pertinently and validated experimentally on both material and processing issues and their overall effects.[78,79]

Because of the explicit demands, studies of wavelength-extended InGaAs FPAs were recently accelerated. For example, Arslan *et al.* reported SSMBE grown 640×512 FPA of 20 μm pitch in 2014,[80] with a cut-off wavelength about 2.65 μm at RT. Mushini *et al.* reported the MOVPE grown 320×256 FPA of 12.5 μm pitch in 2016.[81] The format has reached 1280×1024 with 12-μm pitch reported by Ettenberg *et al.*,[82] which is also an MOVPE grown InAsP/InGaAs system. In the case of MOVPE grown structure with multi-composition steps and large thickness of the buffer layer, the misfit dislocation in the upper active layers could be restrained sufficiently, and under this condition the planar-type device with using diffusion to form pn junction resulted in moderate performance, as reported by Huang *et al.*[83] Compared with InP substrates, GaAs substrates are large in size and cheap in price, which is attractive for mass production. However, the lattice mismatch increases about 4% more for the InGaAs with the same indium content, which can further depredate the performance of the device. The work on $In_xGa_{1-x}As$ PDs and FPAs of $x > 0.53$ on GaAs substrate are still done recently by using MBE and MOVPE, including our work[84–87] and those of other groups.[88,89] The main purpose is to gain the knowledge of higher lattice mismatch. Comparing with the InP-based devices, the performance of GaAs-based device is still poor especially at lower operation temperatures, which makes it only suitable for some low-end applications at RT.

4. Conclusion

The high-spectral-contrast 1 μm–3-μm SWIR band possesses conspicuous spectral sensing and imaging applications, which accelerates the development of PDs and FPAs in this band adopting different material systems, among which the ternary InGaAs on InP substrate has become the most powerful competitor due to its advantageous characteristics and matured technology that is inherited from optical fiber communication. From the background and the brief review of the development of both lattice-matched and wavelength-extended InGaAs PDs and FPAs, it can be concluded that the lattice-matched devices have become matured towards products, immediately followed by wavelength-extended devices.

References

[1] Rogalski A 2001 *Proc. SPIE* **4355** 1
[2] Zhang Y G, Zhou P, Chen H Y and Pan H Z 1990 *Chin. J. Rare Met.* **9** 48
[3] Zhang Y G, Zhou P, Shan H K and Pan H Z 1992 *Chin. J. Semicond.* **13** 623
[4] Afrailov M A 2010 *Infrared Phys. & Technol.* **53** 29
[5] Piotrowski T T, Piotrowska A, Kaminska E, Piskorski M, Papis Golaszewska E K, KtCki J, Ratajczak J, Adamczewsk J, Wawro A, Piotrowski J, Orman Z, Paw1uczyk J and Nowak Z 2001 *Proc. SPIE* **4413** 339
[6] Bhagwat V, Xiao Y G, Bhat I, Dutta P, Refaat T F, Abedin N and Kumar V 2006 *J. Electron. Mater.* **35** 1613
[7] Li A Z, Zhong J Q, Zheng Y L, Wang J X, Ru G P, Bi W G and Qi M 1995 *J. Cryst. Growth.* **150** 1375
[8] Liang B L, Chen D Y, Wang B, Kwasniewski T A and Wang Z G 2010 *IEEE Trans. Electron. Dev.* **57** 361
[9] Sun Y Y, Han X, Hao H Y, Jiang D W, Guo C Y, Jiang Z, Lv Y X, Wang G W, Xu Y Q and Niu Z C 2017 *Infrared Phys. & Technol.* **82** 140
[10] Cohen-Elias D, Uliel Y, Klin O, Snapi N, Weiss E, Shafir I, Westreich O and Katz M 2017 *Infrared Phys. & Technol.* **84** 82
[11] Pearsall T P and Hopson R W 1977 *J. Appl. Phys.* **48** 4407
[12] Pearsall T P 1978 *J. Electron. Mater.* **7** 133
[13] Onat B M, Huang W, Masauna N, Lange M, Ettenberg M H and Driesa C 2007 *Proc. SPIE* **6542** 65420L
[14] Li X, Tang H J, Fan G Y, Liu D F, Shao X M, Zhang Y G, Zhang H Y, Chen X Y, Zhu S G, Gong H M and Fang J X 2007 *Proc. SPIE* **6835** 683505
[15] MacDougal M, Geske J, Wang C, Liao S R, Getty J and Holmes A 2009 *Proc. SPIE* **7298** 72983F
[16] Rouvié A, Reverchon J L, Huet O, Djedidi A, Robo J A, Truffer J P, Bria T, Pires M, Decobert J and Costard E 2012 *Proc. SPIE* **8353** 835308
[17] Rouvié A, Huet O, Hamard S, Truffer J P, Pozzi M, Decobert J, Costard E, Zécri M, Maillart P, Reibel Y and Pécheur A 2013 *Proc. SPIE* **8704** 880403
[18] Rouvié A , Coussement J, Huet O, Truffer J P, Pozzi M, Oubensaid E H, Hamard S, Chaffraix V and Costard E 2015 *Proc. SPIE* **9451** 945105
[19] Li X, Tang H J, Huang S L, Shao X M, Li T, Huang Z C and Gong H M 2014 *Proc. SPIE* **9220** 92200B
[20] Rutz F, Kleinow P, Aidam R, Heussen H, Bronner W, Sieck A and Walther M 2015 *Proc. SPIE* **9481** 948107
[21] MacDougal M, Hood A, Geske J, Wang J, Patel F, Follman D, Manzo J and Getty J 2011 *Proc. SPIE* **8012** 801221
[22] Yuan P, Chang J, Boisvert J C and Karam N 2014 *Proc. SPIE* **9070** 907007
[23] Fraenkel R, Berkowicz E, Bykov L, Dobromislin R, Elishkov R, Giladi A, Grimberg I, Hirsh I, Ilan E, Jacobson C, Kogan I, Kondrashov P, Nevo I, Pivnik I and Vasserman S 2016 *Proc. SPIE* **9819** 981903
[24] Shao X M, Yang B, Huang S L, Wei Y, Li X, Zhu X L, Li T, Chen Y and Gong H M 2017 *Proc. SPIE* **10404** 104040D
[25] Anchlia A, Vinella R M, Gielen D, Wouters K, Vervenne V, Hooylaerts P, Deroo P, Ruythooren W, De Gaspari D, Das J and Merken P 2016 *Proc. SPIE* **9819** 981907
[26] Song K, Lei J F, Petersen A, Yuan H, Kim J, Kimchi J, Douence V, Starr B, Sundareswaran V and Beletic J W 2018 *Proc. SPIE* **10656** 106560K
[27] Tang H J, Li X, Wang Y J, Duan W B, Shao X M and Gong H M 2014 *Proc. SPIE* **8982** 898229
[28] Itzler M A, Entwistle M, Owens M, Patel K, Jiang X D, Slomkowski K, Rangwala S, Zalud P F, Senko T, Tower J and Ferraro J 2011 *Proc. SPIE* **8033** 80330G
[29] Baba T, Suzuki Y, Makino K, Fujita T, Hashi T, Adachi S, Nakamura S and Yamamoto K 2018 *Proc. SPIE* **10540** 105400L
[30] Islam M, Feng J Y, Berkovich A, Abshire P, Barrows G and Choa F S 2016 *Proc. SPIE* **9819** 98190G
[31] Kim Y H, Lee B W, Ko S Y, Ha C S and Jung H 2018 *Proc. SPIE* **10624** 106241T
[32] Deng H H, Shao H B, Yang B, Huang J, Wang Z L, Li X, Shao X M and Gong H M 2017 *Proc. SPIE* **10462** 1046232
[33] Huang X, Li Tao, Shao X M, Li X and Gong H M 2013 *Proc. SPIE* **8907** 890751
[34] Shao X M, Zhu Y M, Li X, Tang H J, Li T and Gong H M 2014 *Proc. SPIE* **9220** 92200A
[35] Zhu X L, Zhang H Y, Li X, Huang Z C and Mei H 2017 *Proc. SPIE* **10404** 104040E
[36] Mo D F, Liu D F, Yang L Y, Xu Q F and Li X 2013 *Proc. SPIE* **8907** 89073T
[37] Joshi A M and Datta S 2018 *Proc. SPIE* **10641** 106410K
[38] Zhang Y G and Gu Y 2011 *Advances in Photodiodes*, Chapter 17 (Rijeka, Croatia: InTech) pp. 349–376
[39] Martinelli R U, Zamerowski T J and Longeway P A 1988 *Appl. Phys. Lett.* **53** 989
[40] Makita K, Torikai T, Ishihara H and Taguthi K 1988 *Electron. Lett.* **24** 379
[41] Forte-Poisson M A, Brylinski C, Persio J, Hugon X, Vilotitch B and Noble Le C 1992 *J. Cryst. Growth* **124** 782
[42] Zhang Y G, Hao G Q, Gu Y, Zhu C, Li A Z and Liu T D 2005 *Chin. Phys. Lett.* **22** 250
[43] Zhang Y G, Gu Y, Zhu C, Hao G Q, Li A Z and Liu T D 2006 *Infrared Phys. & Technol.* **47** 257
[44] Zhang Y G, Gu Y, Tian Z B, Li A Z, Zhu X R and Zheng Y L 2008 *Infrared Phys. & Technol.* **51** 316
[45] Li C, Zhang Y G, Wang K, Gu Y, Li Hsby and Li Y Y 2010 *Infrared Phys. & Technol.* **53** 173
[46] Zhang Y G, Gu Y, Tian Z B, Li A Z, Zhu X R and Wang K 2009 *Infrared Phys. & Technol.* **52** 52
[47] Zhang Y G, Gu Y, Wang K, Li A Z and Li C 2008 *Semicon. Sci. Technol.* **23** 125029
[48] Gu Y, Zhang Y G, Wang K, Li A Z and Li Y Y 2013 *J. Cryst. Growth* **378** 65
[49] Xi S P, Gu Y, Zhang Y G, Chen X Y, Zhou L, Li A Z and Li Hsby 2015 *J. Cryst. Growth* **425** 337
[50] Fang X, Gu Y, Zhang Y G, Zhou Li, Wang K, Li Hsby, Liu K H and Cao Y Y 2013 *J. Infrared Millim. Waves* **32** 481
[51] Du B, Gu Y, Zhang Y G, Chen X Y, Xi S P, Ma Y J, Ji W Y, Shi Y H, Li X and Gong H M 2016 *J. Cryst. Growth* **440** 1
[52] Gu Y, Zhang Y G, Wang K, Fang X and Liu K H 2012 *Jpn. J. Appl. Phys.* **51** 080205
[53] Ma Y J, Zhang Y G, Chen X Y, Gu Y, Shi Y H, Ji W Y and Du B 2018 *J. Phys. D: Appl. Phys.* **51** 145106
[54] Gu Y, Zhou L, Zhang Y G, Chen X Y, Ma Y J, Xi S P and Li Hsby 2015 *Appl. Phys. Express* **8** 022202
[55] Du B, Gu Y, Chen X Y, Ma Y J, Shi Y H, Zhang J and Zhang Y G 2018 *Jpn. J. Appl. Phys.* **57** 060302
[56] Shi Y H, Zhang Y G, Ma Y J, Gu Y, Chen X Y, Gong Q, Du B and Zhang J, Zhu Y 2018 *Infrared Phys. & Technol.* **89** 72
[57] Chen X Y, Gu Y, Zhang Y G, Ma Y J, Du B, Shi Y H, Zhang J and Zhu Y 2018 *Infrared Phys. & Technol.* **89** 381
[58] Zhou L, Zhang Y G, Gu Y, Chen X Y, Cao Y Y and Li Hsby 2013 *J. Alloys Compd.* **576** 336
[59] Ma Y J, Gu Y, Zhang Y G, Chen X Y, Xi S P, Boldizsar Z, Huang L and Zhou L 2015 *J. Mater. Chem. C* **3** 2872
[60] Zhang Y G, Liu K H, Gu Y, Zhou L, Li HSby, Chen X Y, Cao Y Y and Xi S P 2014 *Semicond. Sci. Technol.* **29** 035018
[61] Zhang Y G, Gu Y, Chen X Y, Ma Y J, Li X, Shao X M, Gong H M and Fang J X 2017 *Infrared Phys. & Technol.* **83** 45
[62] Zhang Y G, Gu Y, Chen X Y, Ma Y J, Li X, Shao X M, Gong H M and Fang J X 2018 *Appl. Opt.* **57** D141
[63] Tennant W E, Lee D, Zandian M, Piquette E and Carmody M 2008 *J. Electron. Mater.* **37** 1406
[64] Zhang K F, Tang H J, Wu X L, Li X, Zhang Y G and Gong H M 2007 *Proc. SPIE* **6835** 683506
[65] Shi M, Li T, Shao X M, Li X, Gong H M 2013 *Proc. SPIE* **8907** 890755
[66] Li X, Li T, Yu C L, Tang H J, Deng S Y, Shao X M, Zhang Y G and Gong H M 2017 *Proc. SPIE* **10404** 104040C
[67] Li T, Zhang K F, Li Y F, Tang H J, Li X and Gong H M 2009 *Proc. SPIE* **7383** 73833Z
[68] Zhu Y M, Deng H H, Wei P, Li X and Gong H M 2011 *Proc. SPIE* **8193** 81933D
[69] Li X, Tang H J, Li T, Wei P, Gong H M and Fang J X 2013 *Proc. SPIE* **8907** 890703
[70] Yan H Z, Tang H J, Deng S Y, Chen G, Shao X M, Li T, Li X and Gong H M 2015 *Proc. SPIE* **9522** 95221X
[71] Deng S Y, Li P, Li T, Li X, Shao X M, Tang H J and Gong H M 2015 *Proc. SPIE* **9674** 967420

[72] Shi M, Shao X M, Tang H J, Li T, Wang Y J, Li X and Gong H M 2014 *Infrared Phys. & Technol.* **67** 197
[73] Li P, Li T, Deng S Y, Li X, Shao X M, Tang H J and Gong H M 2015 *Infrared Phys. & Technol.* **71** 140
[74] Yang J, Shi M, Shao X M, Li T, Li X, Tang N Y, Gong H M, Liu R, Tang H J and Qiu Z J 2015 *Infrared Phys. & Technol.* **71** 272
[75] Gong H M, Li X, Li T, Tang H J, Shi M, Shao X M and Zhang Y G 2014 *Proc. SPIE* **9070** 90700C
[76] Huang X, Li X, Shi M, Tang H J, Li T, Shao X M and Gong H M 2015 *Infrared Phys. & Technol.* **71** 514
[77] Kleipool Q L, Jongma R T, Gloudemans A M S, Schrijver H, Lichtenberg G F, Hees R M, Maurellis A N and Hoogeveen R W M 2007 *Infrared Phys. & Technol.* **50** 30
[78] Gu Y, Zhang Y G, Li C, Wang K, Li Hsby, Li X and Fang J X 2011 *Infrared Phys. & Technol.* **54** 497
[79] Li C, Zhang Y G, Gu Y, Wang K, Li Hsby, Li X and Fang J X 2013 *Infrared Phys. & Technol.* **58** 69
[80] Arslan Y, Oguz F and Besikci C 2014 *IEEE J. Quantum Electron.* **50** 957
[81] Mushini P, Huang W, Morales M, Brubaker R, Nguyen T U , Dobies M, Zhang W, Gustus W, Mathews G, Endicter S and Paik N 2016 *Proc. SPIE* **9819** 98190D
[82] Ettenberg M H, Nguyen H, Martin C R and Lange M 2018 *Proc. SPIE* **10624** 1062404
[83] Huang C C, Ho C L and Wu M C 2015 *IEEE Electron Dev. Lett.* **36** 820
[84] Chen X Y, Zhang Y G, Gu Y, Zhou L, Cao Y Y, Fang X and Li Hsby 2014 *J. Cryst. Growth* **393** 75
[85] Zhou L, Zhang Y G, Chen X Y, Gu Y, Li Hsby, Cao Y Y and Xi S P 2014 *J. Phys. D: Appl. Phys.* **47** 085107
[86] Chen X Y, Gu Y, Zhang Y G, Xi S P, Guo Z X, Zhou L, Li A Z and Li Hsby 2015 *J. Cryst. Growth* **425** 346
[87] Chen X Y, Gu Y, Zhang Y G, Ma Y J, Du B, Zhang J, Ji W Y, Shi Y H and Zhu Y 2018 *J. Cryst. Growth* **488** 51
[88] Habchi M M, Tounsi N, Bedoui Zaied M I, Rebey A and Jani B E 2014 *Physica E* **56** 74
[89] Jurczak P, Sablon K A, Gutiérrez M, Liu H Y and Wu J 2017 *Infrared Phys. & Technol.* **81** 320